Proc. Natl. Acad. Sci. USA
Vol. 88, pp. 10801–10805, December 1991
Biochemistry

Structural polymorphism in the major groove of a 5S RNA gene complements the zinc finger domains of transcription factor IIIA

PAUL W. HUBER*, TAKASHI MORII†, HOUNG-YAU MEI‡, AND JACQUELINE K. BARTON†§

*Department of Chemistry and Biochemistry, University of Notre Dame, Notre Dame, IN 46556; †Division of Chemistry and Chemical Engineering, California Institute of Technology, Pasadena, CA 91125; and ‡Department of Chemistry, University of California, Santa Barbara, CA 93106

Communicated by Nicholas J. Turro, July 17, 1991 (received for review May 14, 1991)

ABSTRACT **Metal complexes that bind to DNA on the basis of shape-selection have been used to map the conformational features of the DNA binding site for transcription factor IIIA. Conformationally distinct segments are detected on the 5S rRNA gene that correspond closely to the binding sites identified for the individual zinc finger domains of the protein. The local conformations are characterized by a major groove opened because of a change in base pair inclination and/or displacement at a central 5′-pyrimidine-purine-3′ step, flanked by a widened minor groove, as would arise at the junctions between alternating B- and A-like DNA segments. Docking experiments with a consensus structure of a zinc finger reveal that the mixed A–B binding site accommodates the peptide domain better than either canonical B- or A-DNA helices. The close structural matching of the conformational variations in the 5S rDNA both to the proposed sites of zinc finger binding and to the shape of an individual zinc finger domain points to DNA structural polymorphism as providing an important determinant in recognition. In particular, shape selection in the 5′ half of the internal control region may orient the multiple finger domains.**

With the advent of single-crystal analysis of oligonucleotides, it has become apparent that considerable departures from idealized helix parameters occur in the structure of DNA. Sequence-dependent heterogeneity due to variations in helix twist and base pair roll and tilt have a pronounced effect on the arrangement of the hydrogen bond donors and acceptors of the bases and on the local configuration of the sugar phosphate backbone. Deviations from canonical B-form DNA structure have been observed in the cocrystal structures of several DNA–protein complexes (1–3), and it is likely that such polymorphism in general plays a role in the recognition of nucleic acid sites by proteins.

Metal complexes have been designed that recognize distinct sites along DNA on the basis of shape selection (4–9). These complexes provide sensitive probes for the local variations in helical conformation (10). One advantage of this method of analysis is that structural details in the nucleic acid can be examined in solution under the same conditions used to study protein binding, thereby avoiding conditions that potentially can alter the biologically active structure of the macromolecule. Therefore, such methodology can provide a bridge between the few high-resolution views of short DNA fragments available with NMR spectroscopy and x-ray crystallography and the local sequence-dependent variations in structure that occur on much longer DNA fragments.

Here we apply two of these chiral metal complexes to map variations in the structure of the internal control region (ICR) of the *Xenopus* 5S rRNA gene, which is the binding site for transcription factor IIIA (TFIIIA) (11). This factor contains nine zinc finger domains through which it makes multiple contacts with the gene (12, 13). There have been several experimental observations that have suggested that the structure of the DNA within the ICR is not a canonical B-form helix but instead may be displaced toward the A-form conformation (14–19). In the present experiments we find that the complex $[Ru(Me_4phen)_3]^{2+}$ [for tris(3,4,7,8-tetramethylphenanthroline)ruthenium(II)], which associates preferentially with polynucleotides in the A conformation (6, 20), cuts at several specific regions within the ICR. Immediately adjacent to these sites we find positions cleaved by $[Rh(phen)_2(phi)]^{3+}$ [for bis(phenanthroline)(9,10-phenanthrenequinone diimine)rhodium(III)], which targets sites where the major groove is markedly opened (7, 8). The cumulative results reveal that short segments of A-like conformation may punctuate the binding site for TFIIIA with distinct openings in the major groove occurring at the junctions between the B- and A-type segments. These openings in the major groove correspond closely to the individual finger binding sites identified with deletion mutants of TFIIIA (21) and thus suggest that DNA conformational heterogeneity may be an important element used in orienting the multiple finger domains of the factor along the ICR.

MATERIALS AND METHODS

Nucleic Acids. The plasmid pS18 contains a single copy of a *Xenopus borealis* somatic 5S rRNA gene (17, 22). The plasmid was digested with *Hin*dIII and labeled on the noncoding strand by treatment with alkaline phosphatase followed by rephosphorylation of the 5′ ends with [γ-^{32}P]ATP and polynucleotide kinase. The coding strand was also labeled at the *Hin*dIII site with dideoxynucleotide [α-^{32}P]triphosphate and terminal transferase. After incorporation of the radioactive label, the sample was digested with *Bam*HI and the 248-base-pair (bp) restriction fragment containing the 5S rRNA gene was purified by electrophoresis on a 6% nondenaturing polyacrylamide gel. Sequencing reactions were those of Maxam and Gilbert (23).

Photocleavage Reactions. $[Rh(phen)_2(phi)]Cl_3$ was synthesized, and enantiomers were resolved as described (7, 8). The photocleavage reactions were carried out in solutions containing 20 mM Tris·HCl (pH 7.4), 70 mM KCl, 2 mM $MgCl_2$, and calf thymus DNA (80 μM in nucleotides)—conditions compatible with binding of TFIIIA—and 5 μM rhodium complex. Samples were irradiated with a 1000-W Xe/Hg lamp with a monochromator set at 313 nm for 40 sec at ambient temperature. The samples were then precipitated with ethanol, and the pellets were washed with 70% ethanol to remove the metal complex. $[Ru(Me_4phen)_3]Cl_2$ and tris(phenanthroline)ruthenium(II) chloride $[Ru(phen)_3]Cl_2$

The publication costs of this article were defrayed in part by page charge payment. This article must therefore be hereby marked "*advertisement*" in accordance with 18 U.S.C. §1734 solely to indicate this fact.

Abbreviations: ICR, internal control region; TFIIIA, transcription factor IIIA; $[Ru(Me_4phen)_3]^{2+}$, tris(3,4,7,8-tetramethylphenanthroline)ruthenium(II); $[Ru(phen)_3]^{2+}$, tris(phenanthroline)ruthenium(II); $[Rh(phen)_2(phi)]^{3+}$, bis(phenanthroline)(9,10-phenanthrenequinone diimine)rhodium(III); rDNA, rRNA gene.

§To whom reprint requests should be addressed.

were prepared and characterized as reported earlier (20). The reactions with the ruthenium complexes were carried out in solutions containing 20 mM Tris·HCl (pH 7.4), 70 mM KCl, 2 mM $MgCl_2$, 1.2 mM imidazole, calf thymus DNA (100 μM nucleotides), and 15 μM ruthenium complex. After the irradiation with a He/Cd laser (Liconix) at 442 nm for 20 min, samples were precipitated with ethanol and then treated with 1 M piperidine at 90°C for 30 min. Products of the photocleavage reactions were analyzed by high-resolution polyacrylamide gel electrophoresis. Autoradiographs were scanned using an LKB 2202 Ultrascan laser densitometer interfaced with a Nelson analytical box, and the intensity of each band was converted to a relative probability of cleavage at that site (24). The probability of cleavage by $[Ru(Me_4phen)_3]^{2+}$ at each site was obtained after subtraction of the $[Ru(phen)_3]^{2+}$ cleavage probability to normalize for the differential base reactivity of singlet oxygen.

Molecular Modeling. The mixed A–B DNA binding site model was constructed for a dodecanucleotide based upon the cleavage results with MACROMODEL (W. C. Still) version 2.5. A model zinc finger [coordinates supplied by J. Berg (25)] was docked manually with no nonbonded internuclear distances closer than 3.0 Å. Solvent-accessible surface areas were calculated on MACROMODEL with a probe radius of 1.4 Å.

RESULTS AND DISCUSSION

Mapping Conformational Polymorphism with Shape-Selective Probes. $[Rh(phen)_2(phi)]^{3+}$ binds to duplex DNA by intercalation at positions where the major groove has opened either because of changes in propeller twisting or because of a change in the inclination or displacement of bases towards the major groove (7, 8). This shape selection results from steric interactions between the phenanthroline ligands, which overhang the intercalative phi moiety, and the helical column of base pairs, precluding binding at all sites where the major groove is not open and accessible. Enantiomeric discrimination favoring the Δ-isomer is apparent at sites opened because of a change in propeller twist, while no chiral discrimination is found in sites opened because of variations in base tilt (8). Upon photoactivation, $[Rh(phen)_2(phi)]^{3+}$ cleaves the DNA directly at the bound site without a diffusible intermediate.

Cleavage on the 5S rRNA gene (rDNA) by $[Rh(phen)_2(phi)]^{3+}$ is shown in Fig. 1. On the noncoding strand in the ICR, the principal sites of cutting occur at nucleotides 44–46, 53, 63, 68, 69, 79, 80, 92, and 96. Cleavage is observed at corresponding sites on the coding strand, but is shifted 1 or 2 bp in the 5′ direction. This 5′ asymmetry is consistent with attack without a diffusing intermediate from the major groove (26). While the Λ-isomer cleaves the right-handed DNA with slightly lower overall intensity, no significant chiral discrimination is apparent in cleavage by $[Rh(phen)_2(phi)]^{3+}$ at specific sites (Fig. 1, compare lanes 5 and 6 or 9 and 10), indicating that they must represent junctions where the inclination or displacement of the base pairs (rather than propeller twisting) has opened the major groove. The presence of single distinct sites of cleavage, as opposed to a pattern of cleavage over several base pairs, points to sharp changes rather than the gradual variation that is observed at sites of DNA bending (T.M., unpublished results).

A complementary probe is found in $[Ru(Me_4phen)_3]^{2+}$ that associates with DNA through a surface interaction in regions where the minor groove is both wide and shallow (6, 10, 20). Consequently, this probe reacts most strongly with polynucleotides in the A conformation. The cutting patterns observed with $[Ru(Me_4phen)_3]^{2+}$ are dispersed in comparison to those of the rhodium complex, since cleavage by the former is mediated by singlet oxygen, which is a diffusible species. Also, because singlet oxygen reacts with the DNA bases, preferentially guanines, cleavage patterns with $[Ru(Me_4phen)_3]^{2+}$ must be compared to those of the parent complex, $[Ru(phen)_3]^{2+}$ so as to normalize the inherent sequence selectivity in cleavage associated with a singlet oxygen reaction. The selectivity of $[Ru(Me_4phen)_3]^{2+}$ becomes apparent, since, in addition to some degree of cleavage at all guanine residues, additional sites of cleavage are evident, which reflect regions where the local concentration of singlet oxygen is greater. These are sites where $[Ru(Me_4phen)_3]^{2+}$ is bound preferentially because the minor groove is sufficiently wide and shallow to accommodate the complex.

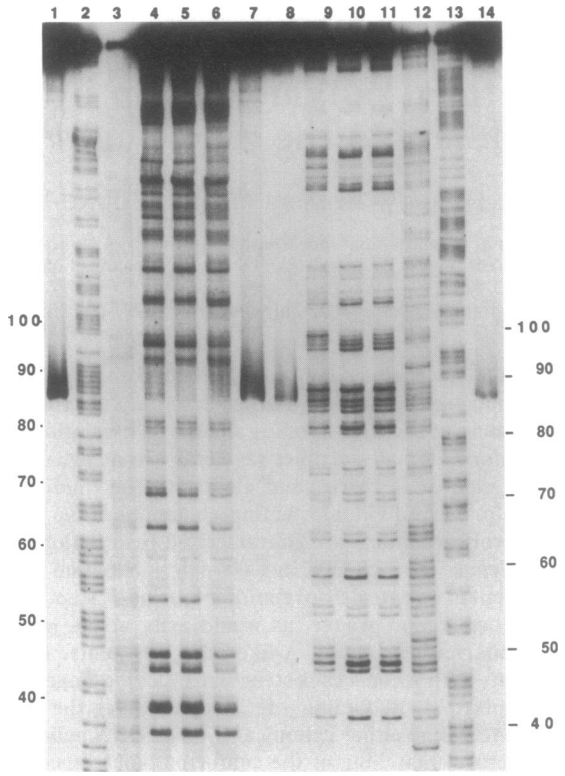

FIG. 1. Openings in the major groove of the ICR determined by photocleavage with $[Rh(phen)_2(phi)]^{3+}$. Autoradiograph showing the *rac*-, Λ-, and Δ-$[Rh(phen)_2(phi)]^{3+}$ photocleavage products from a 248-bp restriction fragment containing a single copy of a *X. borealis* 5S rDNA labeled either on the noncoding (lanes 1–7) or coding (lanes 8–14) strands. Nucleotide positions are marked on the left and right sides of the gel. Lanes: 1 and 14, full fragment without metal complex or irradiation; 2 and 13, the G+A Maxam–Gilbert sequencing reactions; 3 and 12, the C+T sequencing reactions; 4 and 11, photocleavage reactions with *rac*-$[Rh(phen)_2(phi)]^{3+}$; 5 and 10, photocleavage reactions with Δ-$[Rh(phen)_2(phi)]^{3+}$; 6 and 9, photocleavage reactions with Λ-$[Rh(phen)_2(phi)]^{3+}$; and 7 and 8, the full fragment after irradiation without metal present. The smear appearing in control lanes (full undigested fragment) corresponds, based upon isolation and sequencing, to single-stranded full-length DNA that does not remain completely denatured under the conditions of the electrophoresis (see, for example, lane 1 near position 84, or in Fig. 2, lane 6 beginning near position 90).

The cleavage patterns of 5S rDNA cut by $[Ru(phen)_3]^{2+}$ or $[Ru(Me_4phen)_3]^{2+}$ are shown in Fig. 2. The samples irradiated at 442 nm in the presence of $[Ru(phen)_3]^{2+}$ (Fig. 2, lanes 5 and 8) exhibit the characteristic profile for cleavage mediated by singlet oxygen, with cutting occurring predominantly at guanine residues. However, irradiation in the presence of $[Ru(Me_4phen)_3]^{2+}$ (Fig. 2, lanes 4 and 9) reveals additional sites of strong cleavage throughout the 5S rDNA. Within the ICR these sites are centered around nucleotides 44, 50, 56, 76, and 84–90 on the coding strand and at nucleotides 43, 56, 62, 73, 78, 84, and 95 on the noncoding strand. There is a differential reactivity of $[Ru(Me_4phen)_3]^{2+}$ with the two

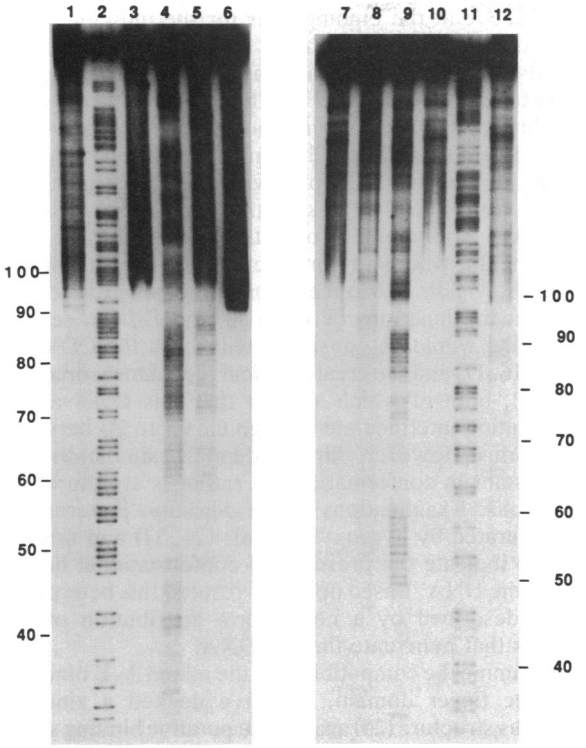

FIG. 2. Regions of A-like structure in the ICR identified by photocleavage with $[Ru(Me_4phen)_3]^{2+}$. Autoradiograph showing the $[Ru(phen)_3]^{2+}$ and $[Ru(Me_4phen)_3]^{2+}$ photocleavage patterns on the restriction fragment containing a single copy of a *X. borealis* 5S rDNA labeled either on the noncoding (lanes 1–6) or coding (lanes 7–12) strands. Lanes: 1 and 12, Maxam–Gilbert C+T sequencing reactions; 2 and 11, the G+A reactions; 3 and 10, the full fragment without metal or irradiation; 4 and 9, photocleavage with $[Ru(Me_4phen)_3]^{2+}$; 5 and 8, photocleavage with $[Ru(phen)_3]^{2+}$; and 6 and 7, irradiation without metal complex present. Cleavage by $[Ru(phen)_3]^{2+}$ is primarily a guanine-specific reaction, while cleavage with $[Ru(Me_4phen)_3]^{2+}$ shows the same guanine reaction on which are superimposed specific regions of cleavage at sites bordering those seen in Fig. 1 with the rhodium complexes.

strands of DNA, suggesting some inherent difference in structure between them.

The combined results with the ruthenium and rhodium probes reveal a remarkable degree of variation in structure across the ICR that is summarized in Fig. 3. The complementary reactivities of the two metal complexes, which probe openings in the major and minor grooves, appear to define repeated G+C-rich elements having the weak consensus sequence 5′-CCTGG-3′. The sites of $[Ru(Me_4phen)_3]^{2+}$ cleavage flank and actually mark the borders of these pentanucleotide sequences, while $[Rh(phen)_2(phi)]^{3+}$ cuts at their center at the 5′-pyrimidine-purine-3′ steps. These elements are dispersed in an irregular pattern along the ICR. Similar cleavage results have also been obtained on DNA fragments consisting only of the 53-bp ICR and a 16-mer (base positions 67–82) (unpublished results). Since the mapping experiments were conducted on linear fragments, this structural heterogeneity cannot be a consequence of the topological constraints in supercoils, but rather it must arise from the sequence of the DNA.

Correlation of Conformational Heterogeneity with Protein Binding. Deletion mutants of TFIIIA have been used in footprinting experiments to locate the binding sites on the gene for all but two of the nine zinc fingers of the protein (21). The results are in agreement with mutagenesis experiments that show that the contacts made by the factor are not uniformly spread across the ICR but are clustered together in three regions (termed boxes A, M, and C) (27). We find a striking correspondence between the repeated structures defined by our conformational probes and the individual finger binding sites mapped with the deletion mutants of TFIIIA (Fig. 3). Strong cleavage sites for $[Rh(phen)_2(phi)]^{3+}$ centered at positions 46, 53, and 59, flanked by cleavage sites for $[Ru(Me_4phen)_3]^{2+}$ were found, for example, at positions indicated for binding by fingers 9, 8, and 7. The G+C-rich elements recognized by the probes centered at positions 64 and 70 correspond to binding sites for fingers 6 and 5. Inherent in the sequence-encoded DNA structure, therefore, appear to be the reoccurring conformational variations necessary to accommodate the zinc finger domains of TFIIIA. The correlation strongly suggests that the zinc finger domains, like our small metal complexes, may recognize these structurally distinct segments through shape selection.

There are several additional points that are noteworthy. First, the distribution of G+C-rich elements along the promoter accommodates the length of the proposed linker sequences between fingers in TFIIIA. Between both fingers 7 and 6 and fingers 6 and 5, for example, the linker lengths are exceptionally short, 5 and 4 amino acid residues, respectively, and we find that the G+C-rich elements that would correspond to binding sites for fingers 7–5 are adjacent one to another. Also, although the pentanucleotide sequence containing a 5′-pyrimidine-purine-3′ step with reinforced stacked purines on each 3′-side appears to generate the local conformation, it is certainly not a requirement from these data that each zinc finger span a full pentanucleotide sequence. Indeed, the sequences of these elements are only weakly conserved in the binding site, but as the amino acid sequence of the individual fingers is only modestly conserved in TFIIIA, there is no reason to expect perfect repeats in the nucleic acid.

The structure of the DNA encompassing the binding sites for fingers 1 and 2 appears to be more complex, particularly in the region from position 85 to position 90, where both probes react with the coding strand. Fairall *et al.* (13) have noted that the distinct periodic methylation of guanine bases

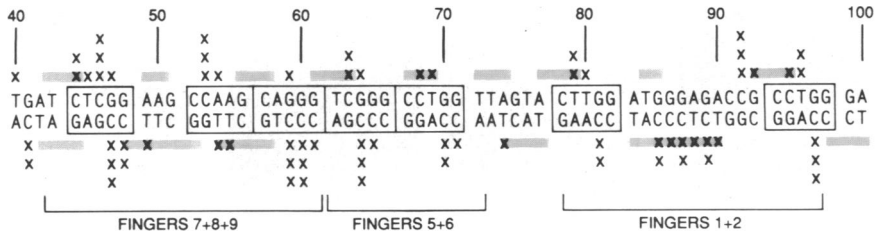

FIG. 3. Conformational map for the internal control region of the *Xenopus* 5S rDNA. Summarized are cleavage probabilities for *rac*-$[Rh(phen)_2(phi)]^{3+}$ (X) and cleavage sites for $[Ru(Me_4phen)_3]^{2+}$ (bars). Also shown are the G+C elements delineated by the cleavage results and the proposed individual finger binding sites determined in studies (21) with TFIIIA deletion mutants. A conformational heterogeneity is clearly apparent across the internal control region. Moreover, a striking correlation between the G+C-rich boxes with open major grooves and sites of zinc finger binding is evident.

in the ICR with dimethyl sulfate is broken at guanosine-85 and -86, which indicates a change in the nature of the interaction within this region. This part of the binding site for TFIIIA contains a cluster of critical contact points for the protein as revealed in methylation interference experiments (28). Thus, the overlapping reactivity of the two probes at this site likely is related to the tight and possibly different mode of binding of TFIIIA to the 3′ end of the ICR (13, 21, 29). In addition, we note that transcription factor IIIC interacts within this segment of the promoter at base pairs 87–89 and also between the G+C boxes at the 5′ end of the ICR at position 51 (30).

The binding of TFIIIA to a series of deletion mutants of the 5S rDNA first indicated that the nature of the interaction between the protein and DNA is not uniform across the ICR (29). Deletions from the 5′ end of the gene up to position 74 exhibited local loss of protection from DNase in footprinting experiments with TFIIIA but still retained some affinity for the protein; more important, these mutants are unable to support transcription. On the other hand, loss of transcription coincided exactly with loss of binding of TFIIIA for deletions made from the 3′ end of the gene. This observation suggests that binding of the factor to the 3′ end of the ICR may be necessary for the additional interactions in the 5′ end that are required to initiate transcription. Moreover, the behavior of mutants of TFIIIA itself also supports the notion that the interaction is not equivalent throughout the region of the gene protected by the factor. Whereas removal of several of the carboxyl-terminal fingers that interact with the 5′-end of the ICR have a moderate effect on binding affinity, removal of the two amino terminal fingers (1 and 2) completely abolish binding (21). Our results indicate that the structural polymorphism of the DNA may dominate the interactions within the 5′ half of the ICR, defining the sites for orientation of the multiple finger domains. This proposal can explain the discrepancy between binding of the factor and initiation of transcription observed with the 5′ deletion mutants, since in the absence of these structural elements, the factor, although attached to the DNA, would not be oriented properly.

Shape Complementarity Between the Major Groove and the Zinc Finger Domain. Nuclease and chemical protection experiments indicate that binding of TFIIIA occurs primarily in the major groove of the DNA (13, 21). The opening up of the major groove at the binding sites for the individual fingers detected with $[Rh(phen)_2(phi)]^{3+}$ supports this proposal and suggests that shape-selection may also serve as a guide in efforts to generate a model for the interaction between the individual zinc finger domains and the DNA helix. From the cleavage data (Fig. 3), the binding site contains a localized opening of the major groove with shallow minor groove elements immediately flanking the open region. Repeated elements of A-form and B-form structure would satisfy these requirements, where an abrupt change in the inclination of the bases, yielding an opening in the major groove, would represent the junctions between A- and B-form segments. This model would be consistent with both the CD spectral results (16, 17) and the greater helical repeat measured for the ICR (17), both of which suggest that this DNA adopts a conformation intermediate (though closer to B) between A- and B-forms. However, our data demonstrate that the ICR is not constant in conformation but rather is structurally heterogeneous. Examinations of the digestion patterns of the ICR generated by hydroxyl radicals (21, 31) and uranyl ion (32) also indicate the presence of conformational heterogeneity in the DNA. Based upon our results, this heterogeneity can be described by a nonuniform distribution of A-like elements that punctuate the 5S rDNA.

To examine the compatibility of the mixed A–B binding site to a zinc finger domain, we have docked a zinc finger consensus structure (25) against the putative binding site. The motif consists of an amphipathic α-helix packed against two antiparallel β-strands that form a compact structure with a hydrophobic interior and several polar side chains on the exterior of the folded peptide (25, 33, 34). Fig. 4*A* shows different views of a Corey–Pauling–Koltun model for the mixed A–B binding site as well as the same site with the zinc finger domain docked in the major groove in Van der Waals contact (the closest nonbonded internuclear distances are $\geq$3Å). The purple and the green atoms designate the α-helix and β-strands, respectively, of the finger, with the yellow atoms marking the amino and carboxyl termini of the domain. The mixed A–B binding site matches and accommodates well the zinc finger domain. Also shown for comparison (Fig. 4 *B* and *C*) are B- and A-form helices with and without the zinc finger domains docked in an analogous fashion. In the case of the A-form helix, the peptide domain appears to be too bulky

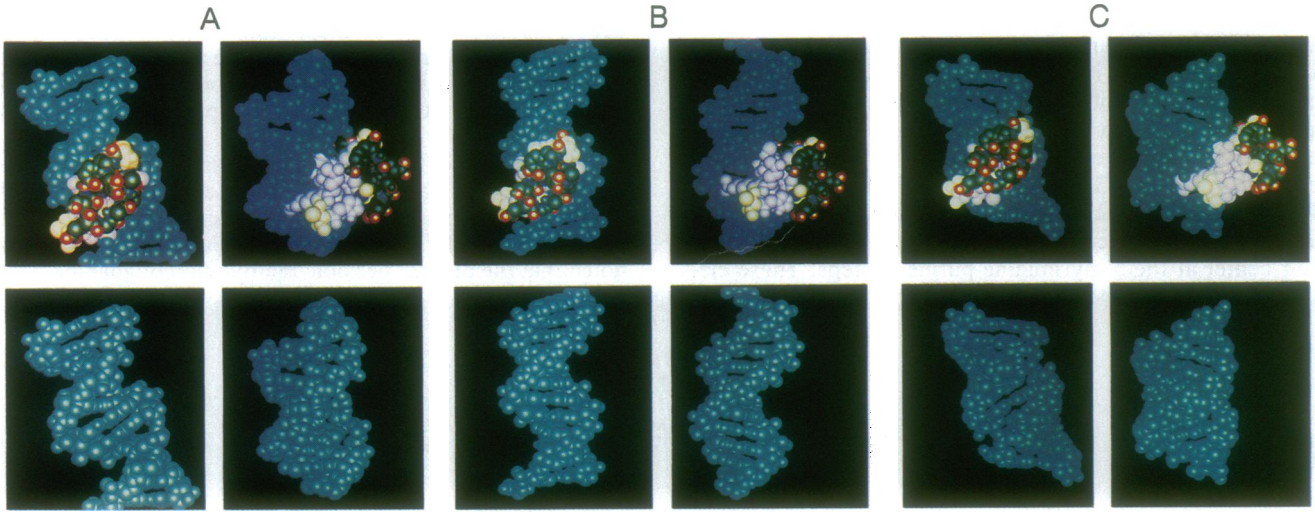

FIG. 4. Docking experiments with a zinc finger domain. Corey–Pauling–Koltun space-filling models of the mixed A–B junction (*A*), uniform B-form (*B*), and uniform A-form (*C*) helices in the presence and absence of a consensus zinc finger. *A–C* show the front view (*Left*) and side view (*Right*) of a dodecamer in the presence (*Upper*) and absence (*Lower*) of bound peptide. The α-helical region of the peptide is shown in purple with the amino and carboxyl termini denoted in yellow. The mixed A–B binding site model has been constructed based upon the cleavage results summarized in Fig. 3 by using MACROMODEL version 2.5. A model zinc finger has been docked manually so that the α-helical region lies in the base pair tilted step.

Table 1. Solvent-accessible surface areas (Å^2) for different DNA-binding models

	DNA*	Peptide domain†	DNA–peptide complex‡	Δ§
A–B junction	3362	1568	3850	1081
B-DNA	3350	1568	3870	1049
A-DNA	3199	1568	3668	1064

Solvent-accessible surface areas (SASA) were calculated by using the program MACROMODEL 2.5 with water (1.4-Å radius) as a probe.
*SASA calculated for the 12-bp DNA fragments depicted in Fig. 4.
†SASA calculated for the individual zinc finger peptide domain.
‡SASA calculated for the DNA–peptide complex depicted in Fig. 4.
§The sum of the surface areas of the DNA and peptide domain minus the surface area of the DNA–peptide complex.

to fit closely against the surface of the major groove, which is too narrow to accept (at reasonable Van der Waals distance) even one side of the α-helical region of the zinc finger. The B-form major groove, in contrast, easily accommodates the full zinc finger, but in this case, the groove dimensions are actually too large, and it is not evident that the peptide domain could make significant contact with both strands simultaneously; the peptide domain cannot span the entire width of the B-form major groove. Instead, if the groove were opened centrally but were somewhat pinched, as occurs at the junction of the mixed A–B model, the structures of the zinc finger domain and the DNA major groove become well matched. This surface complementarity can be quantitated through calculations of the surface areas in these models which are accessible to solvent. The difference in surface area between free and bound complexes is largest for the mixed A–B model and smallest for the B-form structure (Table 1), consistent with the notions seen qualitatively in Fig. 4. Hence, the surface overlap between peptide and nucleic acid is largest for the mixed A–B form, supporting the good structural matching with this model.

There are, however, alternative ways in which one might consider docking the zinc finger domain against the DNA major groove. In the orientation displayed, the α-helix lies along the major groove with the two termini aligned so that neighboring fingers may be easily linked along the major groove. In an alternate orientation, the tip of the domain could instead penetrate the major groove to make sequence-specific contacts, such that amino acid residues towards the base of the finger would be aligned to interact with the ribose phosphate backbone. The linker region can either track along the major groove or cross over into the minor groove depending upon the orientation. As defined by the metal probes, the shape and size of the DNA helix cannot be used to differentiate between these two models. In fact, both modes may be utilized by individual fingers of TFIIIA (21, 31).

Does the A–B junction model realistically reflect the detailed conformation of the nucleic acid bound by a zinc finger peptide domain? Our results define the structural polymorphism inherent in the free nucleic acid; however, CD spectra taken of the 5S gene (17) and the ICR (15) are unchanged in the presence of TFIIIA, suggesting that this heterogeneity is not attenuated by the factor, and may, in fact, play a significant role in determining site recognition. The close structural matching of the peptide domains to an A–B junction and the correspondence of finger binding sites to the centers of these junctions lend strong support to this notion.

Note. Since this manuscript was submitted for publication, the crystal structure of the Zif protein bound to its cognate site has been reported (35). The orientation of the three fingers with respect to the helix is comparable to that shown in Fig. 4. The DNA helical structure, while primarily B-form, also shows an opening toward the major groove at each central 5′-pyridine-purine-3′ step.

We thank Prof. J. Berg for supplying the coordinates of his consensus zinc finger domain. We are grateful for the financial support of the National Institutes of Health (GM33309 and CA33620 to J.K.B.; GM38200 to P.W.H.), the American Heart Association, Indiana Affiliate (Grant in Aid to P.W.H.), and for a Jesse H. Jones Faculty Research Award (to P.W.H.).

1. Otwinowski, Z., Scheritz, R. W., Zhang, R.-G., Lawson, C. L., Joachimiah, A., Marmarstein, R. Q., Luisi, B. F. & Sigler, P. B. (1988) *Nature (London)* **335,** 321–329.
2. Anderson, J. E., Ptashne, M. & Harrison, S. C. (1987) *Nature (London)* **326,** 846–852.
3. McClarin, J. A., Frederick, C. A., Wang, B.-C., Greene, P., Boyer, H. W., Grable, J. & Rosenberg, J. M. (1986) *Science* **234,** 1526–1541.
4. Barton, J. K. (1986) *Science* **233,** 727–734.
5. Kirshenbaum, M. R., Tribolet, R. & Barton, J. K. (1988) *Nucleic Acids Res.* **16,** 7948–7960.
6. Mei, H.-Y. & Barton, J. K. (1988) *Proc. Natl. Acad. Sci. USA* **85,** 1339–1343.
7. Pyle, A. M., Long, E. C. & Barton, J. K. (1989) *J. Am. Chem. Soc.* **111,** 4520–4522.
8. Pyle, A. M., Morii, T. & Barton, J. K. (1990) *J. Am. Chem. Soc.* **112,** 9432–9434.
9. Chow, C. S. & Barton, J. K. (1990) *J. Am. Chem. Soc.* **112,** 2839–2840.
10. Chow, C. S. & Barton, J. K. (1991) *Methods Enzymol.*, in press.
11. Engelke, D. R., Ng, S.-U., Shastry, B. S. & Roeder, R. G. (1980) *Cell* **19,** 717–728.
12. Miller, J., McLachlan, A. D. & Klug, A. (1985) *EMBO J.* **4,** 1609–1614.
13. Fairall, L., Rhodes, D. & Klug, A. (1986) *J. Mol. Biol.* **192,** 577–591.
14. Rhodes, D. & Klug, A. (1986) *Cell* **46,** 123–132.
15. Gottesfeld, J. M., Blanco, J. & Tennant, L. L. (1987) *Nature (London)* **329,** 460–462.
16. Fairall, L., Martin, S. & Rhodes, D. (1989) *EMBO J.* **8,** 1809–1817.
17. Huber, P. W., Blobe, G. C. & Hartmann, K. M. (1991) *J. Biol. Chem.* **266,** 3278–3286.
18. McCall, M., Brown, T., Hunter, W. N. & Kennard, O. (1986) *Nature (London)* **322,** 661–664.
19. Aboul-ela, F., Varani, G., Walker, G. T. & Tinoco, I. (1988) *Nucleic Acids Res.* **16,** 3559–3572.
20. Mei, H.-Y. & Barton, J. K. (1986) *J. Am. Chem. Soc.* **108,** 7414–7416.
21. Vrana, K. E., Churchill, M. E. A., Tullius, T. D. & Brown, D. D. (1988) *Mol. Cell. Biol.* **8,** 1684–1696.
22. Smith, D. R., Jackson, I. J. & Brown, D. D. (1984) *Cell* **37,** 645–652.
23. Maxam, A. M. & Gilbert, W. (1980) *Methods Enzymol.* **65,** 499–560.
24. Lutter, L. C. (1978) *J. Mol. Biol.* **124,** 391–420.
25. Berg, J. M. (1988) *Proc. Natl. Acad. Sci. USA* **85,** 99–102.
26. Dervan, P. B. (1986) *Science* **232,** 464–471.
27. Pieler, T., Hamm, J. & Roeder, R. G. (1987) *Cell* **48,** 91–100.
28. Sakonju, S. & Brown, D. D. (1982) *Cell* **31,** 395–405.
29. Sakonju, S., Brown, D. D., Engelke, D., Ng, S.-Y., Shastry, B. S. & Roeder, R. G. (1981) *Cell* **23,** 665–669.
30. Majowski, J., Mentzel, H. & Pieler, T. (1987) *EMBO J.* **6,** 3057–3063.
31. Churchill, M. E. A., Tullius, T. D. & Klug, A. (1990) *Proc. Natl. Acad. Sci. USA* **87,** 5528–5532.
32. Neilsen, P. E., Mollegaard, N. E. & Jeppesen, C. (1990) *Nucleic Acids Res.* **18,** 3847–3851.
33. Parraga, G., Horvath, S. J., Eisen, A., Taylor, W. E., Hood, L., Young, E. T. & Klevit, R. E. (1988) *Science* **241,** 1489–1492.
34. Lee, M. S., Gippert, G. G., Soman, K. V., Case, D. A. & Wright, P. E. (1989) *Science* **245,** 635–637.
35. Pavletich, N. P. & Pabo, C. O. (1991) *Science* **252,** 809–817.